Cell Reports
Medicine

Article

The gut microbiome regulates the clinical efficacy of sulfasalazine therapy for IBD-associated spondyloarthritis

Graphical abstract

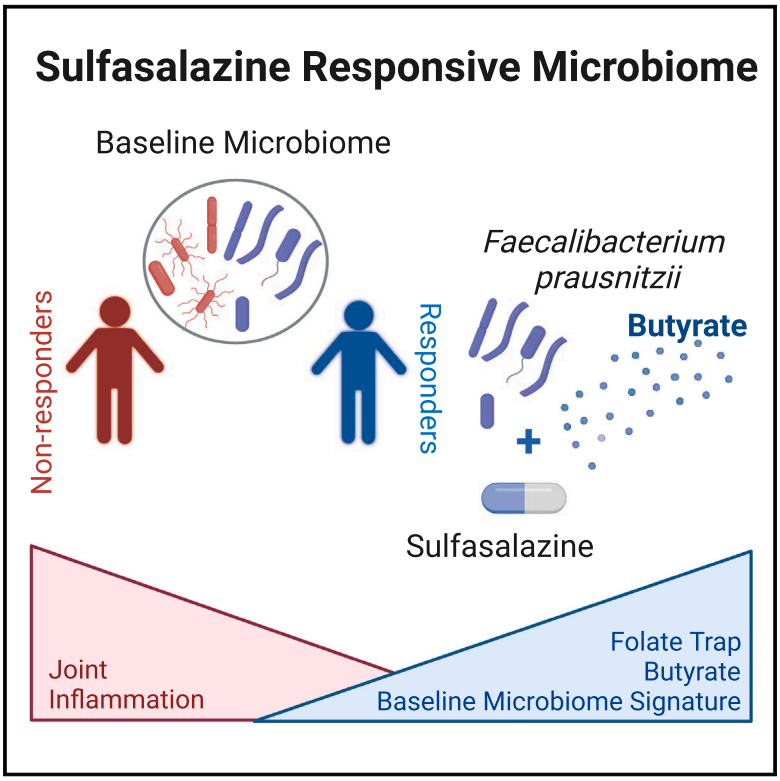

Highlights

- IBD-SpA subjects that respond to sulfasalazine therapy have a distinct gut microbiome
- The responder microbiome is enriched in *F. prausnitzii* and butyrate
- Sulfapyridine promotes butyrate production by *F. prausnitzii*, which limits colitis
- *F. prausnitzii* restores response in mice with non-responder microbiomes

Authors

Svetlana F. Lima, Silvia Pires, Amanda Rupert, ..., Lisa A. Mandl, Ellen J. Scherl, Randy S. Longman

Correspondence

ral2006@med.cornell.edu

In brief

Lima and Pires et al. identified a unique gut microbiome in patients with IBD-associated spondyloarthritis that respond to sulfasalazine therapy. Sulfasalazine therapy enhances butyrate synthesis by *F. prausnitzii*, a key component of this microbiome, which is sufficient to restore sulfasalazine protection from colitis in gnotobiotic mice colonized with non-responder microbiomes.

Lima et al., 2024, Cell Reports Medicine *5*, 101431
March 19, 2024
https://doi.org/10.1016/j.xcrm.2024.101431

CellPress

Cell Reports Medicine

CellPress
OPEN ACCESS

Article

The gut microbiome regulates the clinical efficacy of sulfasalazine therapy for IBD-associated spondyloarthritis

Svetlana F. Lima,[1,2,5] Silvia Pires,[1,2,5] Amanda Rupert,[2,3] Seun Oguntunmibi,[1,2] Wen-Bing Jin,[1] Andrew Marderstein,[1] Gabriela Funez-dePagnier,[2,3] Grace Maldarelli,[1,2] Monica Viladomiu,[1,2] Gregory Putzel,[1] Wei Yang,[1,2] Nancy Tran,[2,3] Grace Xiang,[2,3] Alex Grier,[1] Chun-Jun Guo,[1] Dana Lukin,[2,3] Lisa A. Mandl,[4] Ellen J. Scherl,[2,3] and Randy S. Longman[1,2,3,6,*]

[1]Jill Roberts Institute for Research in IBD, Weill Cornell Medicine, New York, NY 10065, USA

[2]Division of Gastroenterology and Hepatology, Department of Medicine, NewYork-Presbyterian Hospital/Weill Cornell Medical Center, New York, NY 10065, USA

[3]Jill Roberts Center for IBD, NewYork-Presbyterian Hospital/Weill Cornell Medical Center, New York, NY 10065, USA

[4]Division of Rheumatology, Hospital for Special Surgery and Department of Medicine, NewYork-Presbyterian Hospital/Weill Cornell Medical Center, New York, NY 10065, USA

[5]These authors contributed equally

[6]Lead contact

*Correspondence: ral2006@med.cornell.edu

https://doi.org/10.1016/j.xcrm.2024.101431

SUMMARY

Sulfasalazine is a prodrug known to be effective for the treatment of inflammatory bowel disease (IBD)-associated peripheral spondyloarthritis (pSpA), but the mechanistic role for the gut microbiome in regulating its clinical efficacy is not well understood. Here, treatment of 22 IBD-pSpA subjects with sulfasalazine identifies clinical responders with a gut microbiome enriched in *Faecalibacterium prausnitzii* and the capacity for butyrate production. Sulfapyridine promotes butyrate production and transcription of the butyrate synthesis gene *but* in *F. prausnitzii in vitro*, which is suppressed by excess folate. Sulfasalazine therapy enhances fecal butyrate production and limits colitis in wild-type and gnotobiotic mice colonized with responder, but not non-responder, microbiomes. *F. prausnitzii* is sufficient to restore sulfasalazine protection from colitis in gnotobiotic mice colonized with non-responder microbiomes. These findings reveal a mechanistic link between the efficacy of sulfasalazine therapy and the gut microbiome with the potential to guide diagnostic and therapeutic approaches for IBD-pSpA.

INTRODUCTION

Peripheral (pSpA) and axial spondyloarthritis (SpA) are the most commonly reported extra-intestinal manifestations of inflammatory bowel disease (IBD). Using diagnostic criteria established by the Assessment of Spondyloarthritis International Society (ASAS), population cohorts estimate an 8% and 12% prevalence of concomitant axial SpA or pSpA, respectively, in patients with IBD.[1,2] Limitations in the characterization of SpA disease activity in IBD cohorts has led to significant heterogeneity in the estimates of disease prevalence.[3–7] Furthermore, evidence supporting distinct genetic, cellular, and microbial factors that overlap between IBD and SpA highlights the potential for IBD-associated SpA as a separate clinicopathologic entity[8]; however, a better understanding of this biology is needed to guide more targeted and effective use of therapy.

Characteristic alterations in the intestinal microbiome associated with IBD are thought to be a contributor to SpA. Although clinical studies did not validate early associations of SpA with *Klebsiella* sero-reactivity, recent studies using advanced sequencing technology to provide a more complete microbiome analysis have identified potential microbial signatures in subjects with IBD-SpA.[9–11] Specifically, adherent-invasive *Escherichia coli* isolates were found to be expanded in Crohn's-associated pSpA[12] and have been shown to promote T cell inflammation.[13] Moreover, gut dysbiosis in primarily HLA-B27-positive patients with SpA was characterized by decreased microbial diversity, reduced *Faecalibacterium prausnitzii*, and increased levels of *Ruminococcus gnavus* that correlated with SpA disease activity in a subset of patients with a history of IBD.[11,14]

Sufasalazine (SAS) is one of the earliest medications to demonstrate efficacy for induction and maintenance therapy in IBD.[15–18] SAS was designed as a prodrug that consists of sulfapyridine (SP) and 5-aminosalicylate (5-ASA) linked by a diazo bond, which prevents absorption in the proximal intestine.[19] Azoreductases produced by the colonic microbiota cleave the diazo bond and release SP and 5-ASA into the large intestine.[20] While SP can be absorbed and may lead to systemic side effects, 5-ASA remains in the intestine and promotes mucosal healing[21,22]; however, SAS, and not 5-ASA alone, is effective for the treatment of peripheral symptoms of SpA.[23]

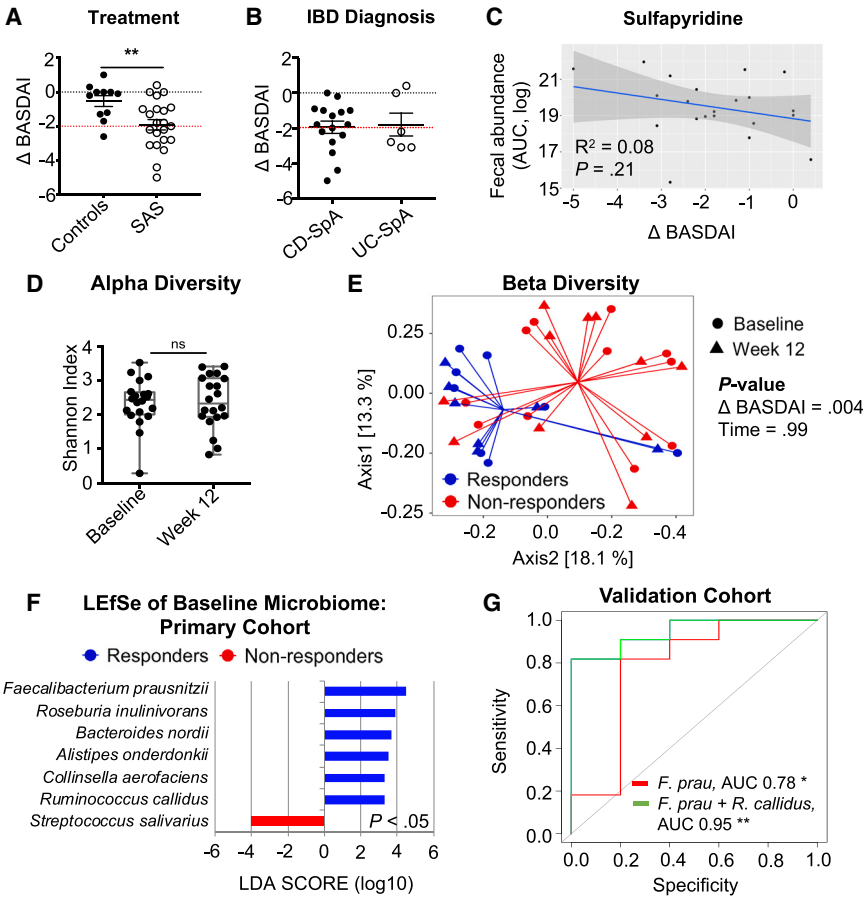

Figure 1. The gut microbiome stratifies sulfasalazine (SAS) BASDAI responders from non-responders with IBD-pSpA

(A and B) Mean Δ BASDAI between baseline and week 12 of controls compared to SAS treatment (A) and SAS treatment stratified by IBD diagnosis of Crohn's disease (CD) or ulcerative colitis (UC). (B) Red line represents the cutoff defining clinical response. Error bars represent the SEM. **p ≤ 0.01, t test.

(C) Linear correlation between fecal abundance of sulfapyridine (SP) and Δ BASDAI.

(D) Boxplots comparing alpha diversity, based on Shannon index, between baseline and week 12. Wilcoxon matched-pairs signed-rank test was not significant (ns).

(E) Principal-coordinate analysis plot is shown using Bray-Curtis and stratified by BASDAI clinical response and time of sample collection. Monte Carlo, permutational multivarate analysis of variance (PERMANOVA) p values are shown.

(F) Bar plot displays the differentially abundant microbial species between responders and non-responders identified by LEfSe at baseline ($p < 0.05$, Mann-Whitney). Modules with a linear discriminant analysis (LDA) score >2 are plotted.

(G) ROC curves demonstrating the ability of the indicated bacterial taxa in discriminating responders from non-responders in a separate validation cohort (n = 16). AUC is indicated. *p ≤ 0.05 and **p ≤ 0.01.

The antibacterial capability of SP to disrupt bacterial synthesis of folate has led to the hypothesis that the microbiome may be critical for understanding the efficacy of SAS. Early studies in patients with rheumatoid arthritis[24] and mouse models[25] highlight the potential effects of SAS on the intestinal microbiome. Sulfamethoxazole, a drug with a similar mode of action to SP, was recently found to modulate *E. coli* metabolic capacity via folate stress, leading to the production of bacterial secondary metabolites with anti-inflammatory properties.[26] However, the impact of the microbiome on the efficacy of SAS therapy for IBD-pSpA has not yet been explored.

In the current study, we prospectively assess the clinical and microbiome characteristics associated with the efficacy of SAS therapy in subjects with active IBD-associated pSpA (IBD-pSpA). The Bath Ankylosing Spondylitis Disease Activity Index (BASDAI), a patient-reported tool that has been clinically validated for the assessment of inflammatory activity and responsiveness to therapy in axial SpA[12,27,28] and pSpA,[29] reveals a higher rate of clinical response and absolute score reduction in SAS-treated subjects compared to controls. Fecal microbiome analysis reveals a baseline gut bacterial signature associated with this clinical response in joint symptoms. Metabolic and transcriptional profiling identifies the mechanistic regulation of microbial butyrate production by SAS in *F. prausnitzii*, the key taxa associated with clinical response. These results highlight the role for drug-microbiome interactions in regulating the clinical efficacy of SAS therapy for IBD-pSpA and provide a clinical model for further investigation of the biology of IBD-SpA as a distinct clinicopathologic entity.

RESULTS

BASDAI identifies clinical response in joint symptoms to SAS in IBD-pSpA

Thirty-three sequential patients with a clinical diagnosis of IBD and ASAS-defined SpA were enrolled (Table S1; Crohn's disease [CD] 78.0%, n = 25; ulcerative colitis [UC] 20.0%, n = 8). Twenty-two of the enrolled patients were treated with SAS therapy, while 11, who were either intolerant to or refused SAS therapy, were followed as standard of care controls. No significant differences were found between treatment groups in terms of IBD diagnosis, age, disease duration, Montreal disease locations, HLA-B27 status, or history of surgery; however, the proportion of females enrolled was higher in controls compared to SAS-treated patients (p = 0.054, Table S1). Consistent with previous clinical data showing the efficacy of SAS for pSpA,[23] a significantly higher proportion of patients achieved clinical response in joint symptoms (defined by a reduction in BASDAI of >2) at week 12 in the SAS group compared to controls (45.4% vs. 9.1%, p = 0.04, Table S1). Participants treated with SAS also had a significant absolute score reduction in BASDAI compared to controls (Figure 1A). Another SpA disease

activity index, the Ankylosing Spondylitis Disease Activity Score (ASDAS), includes patient-reported symptoms, a global activity score, and an objective serum marker of inflammation such as C-reactive protein (CRP) or erythrocyte sedimentations rate.[30] A similar trend in clinical response was observed using ASDAS (28.6% vs. 0%, p = 0.07, Table S1; Figure S1A), but no difference in CRP alone was observed (Table S1; Figure S1A). Consistent with concordance between intestinal and pSpA symptoms, a higher proportion of patients receiving SAS had clinical response by the Harvey-Bradshaw Index (HBI) compared to standard of care controls (Table S1, 29.4% vs. 11.1%, p = 0.30; Figure S1A, p = 0.08). The absolute reduction in BASDAI for subjects treated with SAS was similar between CD and UC (Figure 1B). Of the 22 patients treated with SAS, 50% (n = 11) tolerated increase to 4 mg/day; however, participants taking 2 or 4 mg daily had equivalent reductions in BASDAI (Figure S1B). Baseline biologic or mesalamine therapy did not impact the change in disease activity scores following SAS treatment (Figure S1C).

The gut microbiome stratifies IBD-pSpA subjects with clinical response to SAS

Given the higher proportion of IBD-pSpA subjects treated with SAS showing clinical response by BASDAI, we sought to define potential biomarkers associated with this effect. No significant differences were found between SAS responders and non-responders in terms of IBD diagnosis, age, disease duration, Montreal disease locations, HLA-B27 status, or history of surgery (Table S2). In addition to significant BASDAI and ASDAS reduction in responders, a concordant reduction was also seen in intestinal symptoms measured by HBI.

Since SAS is a prodrug, we performed fecal metabolomics to assess intestinal drug conversion. SAS and its cleavage product SP were detected in week 12 fecal samples (Figure S1D). SAS and/or SP were detected in all samples, but the variability in fecal SP may reflect less efficient conversion of prodrug or clearance. To evaluate whether SAS conversion to SP associates with pSpA clinical response, we performed linear regression analysis. There was no significant correlation between SP or 5-ASA fecal levels and Δ BASDAI (Figures 1C and S1E).

With the potential role for SP in regulating the gut bacteria, we next sought to evaluate the possibility that the clinical response of pSpA symptoms to SAS depends on the diversity of the gut microbiome using 16S rRNA sequencing. Although no significant differences in alpha diversity, as measured by Shannon index, were observed between baseline and week 12 (Figure 1D), an increase in alpha diversity correlated with improvement in BASDAI (Figure S1F, p = 0.037).

To determine the microbiome composition and its functional potential, we performed metagenomic sequencing (average reads/sample $\sim 4.0 \times 10^6$, SEM $\pm$ 3.7×10^5 at baseline and $4.6 \times 10^6 \pm 3.3 \times 10^5$ at week 12). Principal-coordinate analysis (PCoA) based on the Bray-Curtis distance derived from the taxa relative abundance was performed to evaluate whether the microbial community was affected by SAS treatment. Although PCoA revealed no differences in the overall microbial structure between baseline and week 12, significant differences were found between the microbial composition of SAS responders compared to non-responders (Figure 1E).

We next sought to determine the baseline taxa associated with clinical response to SAS by using linear discriminant analysis effect size (LEfSe).[31] Six bacterial species, including *Alistipes onderdonkii*, *Bacteroides nordii*, *Collinsella aerofaciens*, *F. prausnitzii*, *Roseburia inulinivorans*, and *Ruminococcus callidus*, were found to be significantly enriched in clinical responders, while *Streptococcus salivarius* was enriched in non-responders (Figure 1F, Mann-Whitney <0.05; Figures S2A and S2B). Microbial markers were stably enriched in responders at week 12 (Figure S2A).

To validate these bacterial taxa as potential markers of sulfasalazine response, we generated a validation cohort using a separate biobank established at Weill Cornell Medicine. We identified 16 subjects with a diagnosis of IBD and SpA that were currently taking sulfasalazine (Table S2). Five subjects had active SpA symptoms and were characterized as non-responders, while 11 subjects had inactive SpA symptoms and were characterized as responders. We performed 16S rRNA sequencing of fecal samples from these subjects. Like the primary cohort, the relative abundance of both *F. prausnitzii* and the combined bacterial taxa were higher in responders compared to non-responders (Figure S2C). We fit logistic regression models and generated receiver operating characteristic (ROC) curves to determine the ability of the relative abundances of our marker taxa (*F. prausnitzii* alone or *F. prausnitzii* + additional taxa) to discriminate responders vs. non-responders in this separate cohort. *F. prausnitzii* had the highest area under the curve (AUC 0.78) of all the taxa identified (Figure 1G). Combining *F. prausnitzii* with *R. callidus* (also identified in the initial cohort enriched in responders) yields ROC curves with an AUC of 0.95 (Figure S2D).

Baseline differences in metabolic pathways and butyrate synthesis stratify SAS responders

The significant differences in baseline microbiome composition between responders and non-responders suggest a potential functional role for the microbiome in response to SAS. To understand the functional potential of the SAS-responsive microbiome, we performed microbial pathway analysis. PCoA based on the Bray-Curtis distance derived from the abundance (counts per million) of microbial pathways revealed significant differences between responders and non-responders (Figure 2A). LEfSe analysis identified 30 microbial pathways differentially abundant between clinical response groups at baseline, of which 22 were enriched in responders (Figure S3A, Mann-Whitney <0.05). The pathways enriched in responders mainly reflected sub-pathways related to basic cellular processes such as carbohydrate degradation (Figures 2B and S3A: 11 pathways marked in bold), which promotes short-chain fatty acid (SCFA) production characteristic of a healthy microbiome.[32] Most of these differences mapped to the butyrate producer *F. prausnitzii* (Figure S3B). Specifically, the glutaryl-CoA degradation pathway (identified by LEfSe as one of the main pathways enriched in responders; pathway 7, Figure 2B) is a main producer of butyryl-CoA, leading to the production of butyrate (Figure 2C).[33,34]

To determine if butyrate production was associated with SAS clinical response, we determined fecal SCFA concentrations for acetate, butyrate, and propionate. Consistent with the

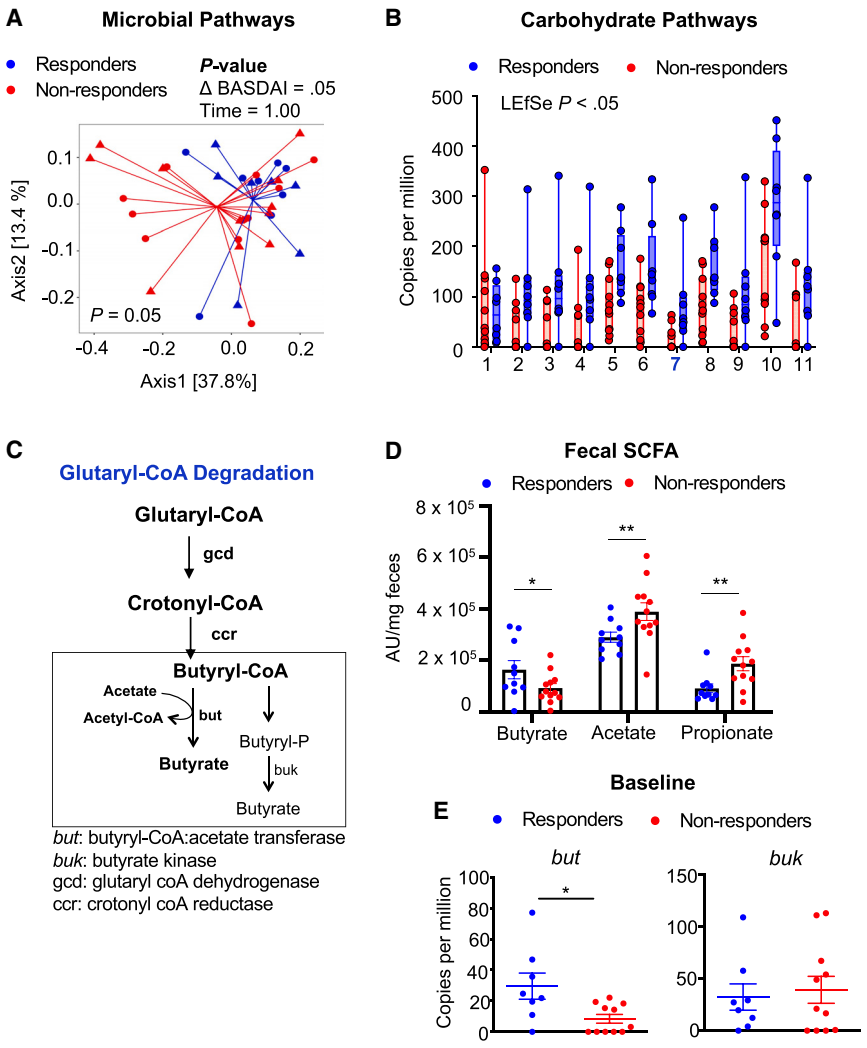

Figure 2. Baseline differences in butyrate synthesis pathway stratify SAS clinical response

(A) Principal-coordinate analysis plot is shown using Bray-Curtis and stratified by BASDAI clinical response and time of sample collection. Monte Carlo, PERMANOVA p values are shown.

(B) Boxplots comparing median carbohydrate degradation sub-pathway abundance (copies per million) between responder and non-responder at baseline (see Figure S3A, marked in bold). 1: dTDP L-rhamnose biosynthesis I; 2: superpathway of hexuronide and hexuronate degradation; 3: D-galacturonate degradation I; 4: superpathway of β-D-glucuronide and D-glucuronate degradation; 5: D-galactose degradation V (Leloir pathway); 6: sucrose degradation III (sucrose invertase); 7: glutaryl-CoA degradation; 8: galactose degradation I (Leloir pathway); 9: four-deoxy-L-*threo*-hex-4-enopyranuronate degradation; 10: starch degradation V; and 11: D-fructuronate degradation. Boxplots present the median, 25th, and 75th percentiles, and Mann-Whitney $p < 0.05$ is shown.

(C) Schematic of butyrate synthesis pathway from glutaryl-CoA degradation. *ccr*, crotonyl-CoA reductase; *gcd*, glutaryl-CoA dehydrogenase; *but*, butyryl-CoA:acetate CoA transferase; *buk*, butyrate kinase.

(D) Relative abundance of fecal short-chain fatty acid was determined by mass spectrometry and normalized per mg fecal sample used. t test, *$p < 0.05$ and **$p < 0.01$ is shown.

(E) Baseline *but* and *buk* mean abundances (copies per million) between responders and non-responders. Error bars represent SEM. *$p < 0.05$, t test.

metagenomic analysis, baseline responders had higher levels of fecal butyrate and lower levels of acetate and propionate compared to non-responders (Figure 2D). While both butyryl-CoA:acetate transferase (*but*) and butyrate kinase (*buk*) can catalyze this reaction, only *but* gene abundance was higher in responders compared to non-responders (Figure 2E). At 90% similarity by UniRef, the *but* gene mapped to *F. prausnitzii*, *Parabacteroides merdae*, *Parabacteroides distasonis*, *Eubacterium rectale*, and *Alistipes shahii* (Figure 3A), but only *F. prausnitzii* was part of the taxa differentiating responders from non-responders.

SP regulates butyrate synthesis and correlates with a folate trap seen in SAS responders

We next tested if SAS was able to modulate this butyrate synthesis pathway in bacteria. Using the lead bacterial taxa *F. prausnitzii* associated with SAS response as a candidate target, we performed bacterial RNA sequencing (RNA-seq) at a sub-inhibitory SP dose of 1 mM, which is within the physiologic range of sulfasalazine in bile excretion (35–1,032 μg/mL)[35] (Figures 3B and S4A). Differential expression analysis of vehicle control (NaOH)- and SP-treated *F. prausnitzii* revealed significant changes in *F. prausnitzii*'s transcription profile upon SP exposure (Figure 3C). The most significant transcriptional targets of SP exposure included downregulation of acetate kinase (*ackA*) and phosphate acetyltransferase (*pta*), along with a concomitant increase in *but* expression (Figure 3D). To test the impact of SP on the metabolic production of butyrate in complete media, mass spectrometry was performed after 22 and 46 h of *F. prausnitzii* culture treated with SP or vehicle control. At both time points, SP treatment robustly increased butyrate production (Figure 3E). To evaluate the specificity of SP on *F. prausnitzii*, we tested the impact of SP on *but* expression in *E. rectale*, the other major contributor to *but* expression in the microbiome. In contrast to *F. prausnitzii*, SP treatment at 1 mM did not change expression of *but* in *E. rectale* (Figures 3F and S4B).

Given the ability of SP to inhibit dihydropteroate synthase (*folP*), we suspected that folate-related stress contributes to the transcriptional regulation by SP observed in the *F. prausnitzii in vitro* assay. In our RNA-seq analysis, we detected a significant downregulation of the *folP*-like enzyme MBL-fold metallohydrolase.[36] In addition, we also observed upregulation

CellPress
OPEN ACCESS

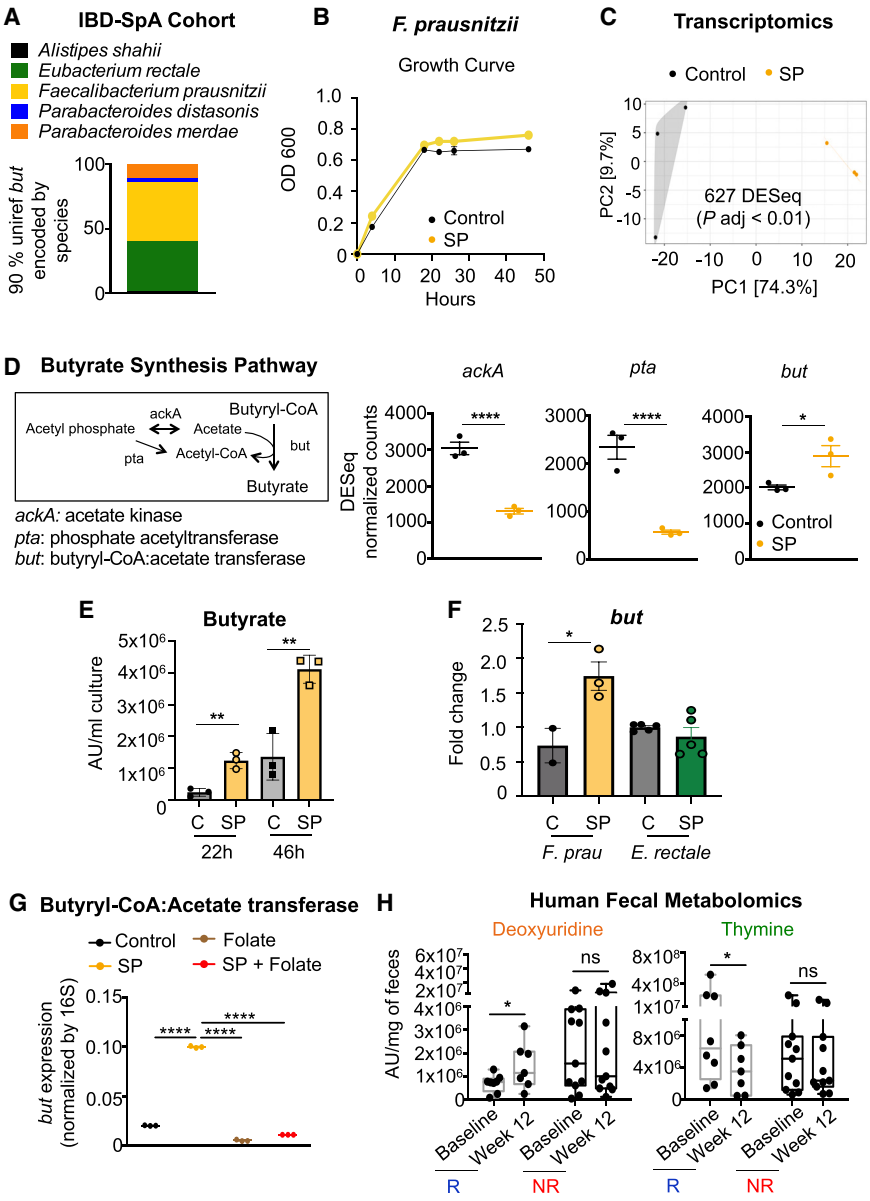

Figure 3. SP-induced folate stress regulates *Faecalibacterium prausnitzii* expression of butyrate synthesis pathway genes

(A) Average percentage of *but* reads from the IBD-pSpA cohort at baseline. Metagenomic sequences aligned by bacterial species based on 90% homology.

(B and C) *F. prausnitzii* grown anaerobically with sub-inhibitory dose of SP (1 mM) or sodium hydroxide vehicle (control [C]) over 46 h.

(C) Principal-component plot from RNA-seq analysis performed at h 46 depicted in (B). On average, four million reads mapped to *F. prausnitzii* (~10× genome coverage).

(D) Schematic highlights pathway and enzymes regulating butyrate synthesis. Normalized counts (log_2 copies per millions) of genes related to the *F. prausnitzii* butyrate synthesis pathway genes. Error bars represent the SEM. *p < 0.05 and ****p < 0.0001, DESeq (p adjusted, false discovery rate [FDR]).

(E) Butyrate abundance measured by mass spectrometry following *in vitro* culture of for 22 or 46 h with either vehicle C or SP treatment as indicated. Technical replicates are shown, **p < 0.01, t test.

(F) Fold change of *but* transcription in either *F. prausnitzii* or *E. rectale* at 22 h with either vehicle C or SP treatment as indicated. Technical replicates are shown, *p < 0.05, t test.

(G) *In vitro F. prausnitzii but* expression was measured at 30 h post-bacteria exposure to SP, folate, and/or sodium hydroxide vehicle (C) by qPCR. Scatterplot error bars represent the SEM. ****p < 0.0001, ANOVA, Tukey's multiple comparison test.

(H) Boxplot comparing the median deoxyuridine and thymine fecal abundance within BASDAI clinical response groups (R, responders; NR, non-responders). Boxplots present the median, 25th, and 75th percentiles; *p < 0.05; Wilcoxon matched-pairs signed-rank test.

in *folC* (dihydrofolate reductase) and *folT* (folate ECF transporter S component) genes consistent with *folP* inhibition (Figure S4C). During reduced availability of folate,[37] thymine is consumed by the salvage pathway, and deoxyuridine subsequently accumulates in bacterial cells (i.e., "folate trap"; Figure S4D). Consistent with this physiology, bacterial cultures showed a significant increase in thymidine kinase expression and a corresponding decrease in thymine metabolites (Figures S4E and S4F).

To directly test the regulation of the *but* gene by folate deficiency, *F. prausnitzii* was cultured with SP or NaOH vehicle control in the absence or presence of supplemental folate, using a dose previously reported to rescue bacteria from antifolate drug treatment[38] (Figure S4G). Consistent with a mechanistic role for folate deficiency, the induction of *but* in response to SP was abrogated by supplementation with folate (Figure 3G). Finally, to test if metabolic evidence of a folate trap correlated with clinical response to SAS, we performed metabolomics analysis on fecal samples from our original cohort. Although all subjects in this study received folate supplementation, dietary folate is primarily absorbed in the small intestine, while SAS prodrug cleavage by microbial azoreductases occurs locally in the colon,[39] enabling the potential for local folate depletion by SP in the colon. Consistent with this possibility and the folate trap effect in the *F. prausnitzii in vitro* model, thymine fecal abundance significantly reduced after SAS treatment in responders (p = 0.016) but not in non-responders (Figure 3H). A concomitant increase in fecal deoxyuridine levels was also observed in responders (p = 0.05) but not in non-responders.

SAS-induced butyrate reduces colitis severity

To determine the functional impact on butyrate synthesis *in vivo,* we treated wild-type (WT) mice with SAS. WT mice received from The Jackson Laboratory were confirmed to have *but* gene

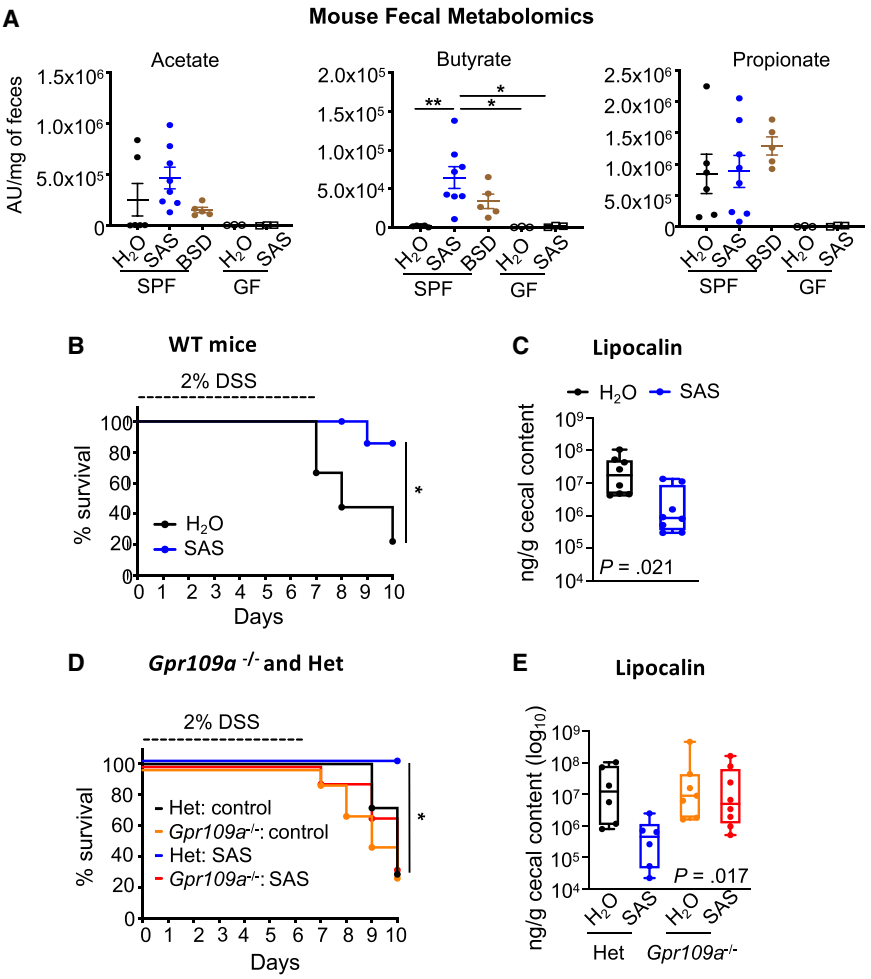

Figure 4. SAS promotes butyrate production and limits colitis

(A) Fecal acetate, butyrate, and propionate levels of germ-free (GF) or Jackson specific-pathogen-free (SPF) mice at day 14 post-treatment initiation with SAS, balsalazide (BSD), or water (H_2O) C. Graphs show data from 2 independent experiments. Error bars represent SEM. **p < 0.01; ANOVA with Tukey's multiple comparison test.

(B and C) Jackson SPF mice were treated with SAS or H_2O vehicle for 7 days and then exposed to 2% DSS *ad libitum* for 7 days. Treatments were maintained throughout the experiment. Percentage of survival (B) and lipocalin (C) are shown. Graph shows data from 2 independent experiments (H_2O, n = 9; SAS, n = 8; BSD, n = 9).

(D and E) SPF *Gpr109a*$^{-/-}$ and heterozygous (Het) littermate controls were treated with SAS or H_2O vehicle for 7 days and then exposed to 2% DSS *ad libitum* for 7 days. SAS treatment was maintained throughout the experiment. Percentage of survival (D) and cecal lipocalin (E) are shown. Graph shows data from 2 independent experiments (Het-H_2O, n = 7; Het-SAS, n = 6; *Gpr109a*$^{-/-}$-H_2O, n = 10; *Gpr109a*$^{-/-}$-SAS, n = 9). Survival analysis; *p < 0.05 and **p < 0.01; log-rank (Mantel-Cox) test. Boxplots present the median, 25th, and 75th percentiles; ANOVA with Kruskal-Wallis multiple comparison test; p values are shown.

containing microbiota (Figure S5A). Although no significant change in acetate or propionate was noted upon SAS treatment, SAS-treated mice had a significant increase in fecal butyrate levels compared to that observed in H_2O vehicle controls (Figure 4A). This effect was dependent on the microbiota, as germ-free mice revealed no changes in fecal butyrate levels post-treatment. Further, to test the role for SP in mediating this effect of SAS, specific-pathogen-free mice were also treated with a related 5-ASA without SP called balsalazide (BSD). Both SAS and BSD prodrugs were efficiently converted by the mouse gut microbiome, as demonstrated by equal 5-ASA detection in fecal samples (Figure S5B). Despite a numerically higher amount of fecal butyrate following BSD, only SAS-treated mice had significantly higher fecal butyrate levels compared to controls.

Given the impact of SAS on microbiota-dependent butyrate production *in vivo*, we next tested the impact of SAS induction of butyrate in an acute model of chemical-induced colitis using dextran sodium sulfate (DSS). SAS treatment significantly reduced mortality (Figure 4B), attenuated weight loss (Figure S5C), and reduced cecal lipocalin (Figure 4C) compared to control-treated mice following DSS-induced colitis. To assess if this effect was dependent on butyrate production, mice deficient for the butyrate receptor Gpr109a and heterozygous controls were used. SAS treatment of mice heterozygous for Gpr109a showed significantly improved survival (Figure 4D), reduced weight loss (Figure S5D), and decreased intestinal inflammation, as measured by cecal lipocalin (Figure 4E), compared to control mice not treated with SAS following exposure to DSS. The effect of SAS was dependent on the butyrate receptor, as mice deficient for Gpr109a showed no effect of SAS on survival (Figure 4D), weight loss (Figure S5D), or inflammation measured by lipocalin (Figure 4E).

F. prausnitzii enhances SAS protection from colitis in non-responder colonized mice

To determine if the IBD-pSpA responder and non-responder microbiomes were sufficient to determine differential response to SAS *in vivo*, gnotobiotic mice were separately colonized with 6 individual donor microbiomes 3 weeks prior to metabolomic analysis (Figure 5A). Consistent with a donor-dependent approach outlined previously,[40] three responder and three non-responder donors were assessed independently with 2–5/mice per donor. Efficient engraftment was determined by beta diversity analysis (Figure S5E). Mice colonized with responder microbiomes showed higher abundance of fecal butyrate following SAS treatment (Figure 5B), while the abundance of butyrate in mice colonized with non-responder microbiome was not changed by treatment with SAS (Figure 5C).

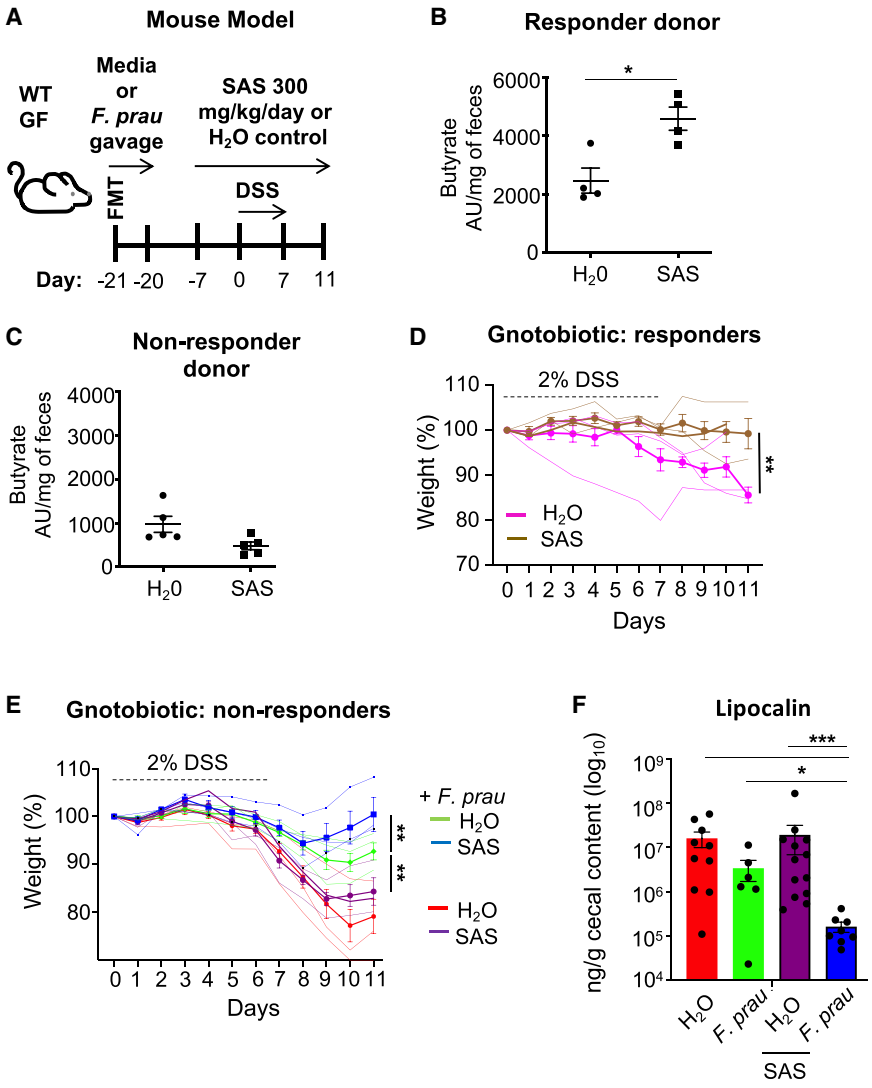

Figure 5. SAS reduces colitis in gnotobiotic mice colonized with responder microbiomes or non-responder microbiomes with *F. prausnitzii*

(A) Schematic of gnotobiotic mouse colonization.

(B and C) Fecal butyrate per mg feces at 7 days after colonization prior to initiation of DSS. One representative of three responders (B) or non-responders (C) is shown as indicated. Error bars represent SEM; *p < 0.05, t test.

(D–F) GF mice received fecal microbial transplants (FMTs) from three responders (D) or three non-responder subjects (E and F). *F. prausnitzii* group was orally gavaged with *F. prausniztii* prior to DSS (E and F). SAS treatment was initiated 14 days post-FMT and maintained throughout the experiment. Mice were exposed to 2% DSS *ad libitum* for 7 days starting 7 days post-SAS initiation. Weight loss and levels of lipocalin in cecal contents are shown (E and F). Graphs show average data (thick line) of three individual donors (thin line). Each thin line is average of n = 3–5 mice/donor. Dark lines are the average and SEM of pooled data from all three donors. Total responder-H_2O, n = 12; responder-SAS, n = 14; non-responder-H_2O, n = 10; non-responder-SAS, n = 13; non-responder + *F. prausnitzii*, n = 9; non-responder-SAS + *F. prausnitzii*, n = 9). Mixed-effects model (weight loss) or Kruskal-Wallis test with multiple comparison (lipocalin). p values are shown. Error bars represent SEM; *p < 0.05, **p < 0.01, and ****p < 0.0001.

To assess the microbiome impact on the SAS response in a colitis model, gnotobiotic mice separately colonized with these 6 individual donor microbiomes were exposed to DSS. Gnotobiotic mice colonized with responder microbiomes from three independent experiments developed weight loss and intestinal inflammation measured by lipocalin, which was reduced by SAS treatment (Figures 5D and S5F). In contrast, gnotobiotic mice colonized with non-responder microbiomes from three independent experiments developed weight loss, which was not responsive to SAS treatment (Figure 5E). To test if *F. prausnitzii* could enhance the response of non-responder microbiome-colonized mice to SAS, we exposed non-responder microbiome-colonized mice to *F. prausnitzii* by oral gavage prior to DSS-colitis induction. Gnotobiotic mice colonized with non-responder microbiomes and exposed to *F. prausnitzii* were responsive to SAS therapy, as demonstrated by reduced weight loss and cecal lipocalin (Figures 5E and 5F). Although *F. prausnitzii* alone reduced the weight loss in non-responder microbiome-colonized mice, *F. prausnitzii* + SAS limited weight loss more dramatically and reduced inflammation measured by lipocalin.

DISCUSSION

Although SpA is the most common extra-intestinal manifestation in IBD, limitations in both diagnostic and therapeutic strategies for IBD-pSpA frequently delay treatment and response rates. Consistent with previously reported studies,[23] we found that SAS therapy leads to improvement in pSpA symptoms of patients with IBD as measured by BASDAI and ASDAS. Even though pSpA can be concordant with intestinal disease activity, SpA symptom improvement did not track with HBI or CRP alone, highlighting the importance of independent evaluation of joint symptoms. Previous studies identified differences in the fecal microbiome of subjects with IBD-SpA compared to SpA alone including the expansion of adherent-invasive *E. coli*[12] and *R. gnavus*.[11] Here, we provide evidence that the baseline microbiome can discriminate responders and non-responders to SAS therapy. Metagenomic analysis revealed distinct baseline gene markers that correlate with SAS response including sub-pathways related to the basic cellular processes of carbohydrate degradation and SCFA synthesis characteristic of a healthy microbiome.[32] The enrichment of the butyrate producers *F. prausnitzii*, *A. onderdonkii*, and *R. inulinivorans* in SAS responders may identify a cohort with higher anti-inflammatory potential for the induction of interleukin-10 or regulatory T cells.[41–43]

F. prausnitzii is the most robust taxa discriminating SAS responders from non-responders in our validation cohort. Consistent with this finding, *F. prausnitzii* has been reported to be reduced in patients with SpA with a history of IBD[14] and may provide a key link between disease biology and SAS response.

The microbiome has long been considered a target of SAS therapy, but the specific taxa and mechanisms involved in drug efficacy have not been defined. Previous studies have suggested that SAS acts as a direct antimicrobial on gut bacteria.[24,25] Recent work also demonstrated an antifolate/antimicrobial effect of methotrexate on gut bacteria.[38] Another possible mechanism is drug metabolism by the microbiome, highlighted by a recent report revealing that microbiome metabolism of 5-ASA stratifies mesalamine responders from non-responders.[44] Here, we do not observe a direct antimicrobial effect of SAS or a differential role for microbiome metabolism of SAS accounting for clinical response. Instead, our study now reveals a mechanism by which SAS acts as a xenobiotic on *F. prausnitzii* to modulate transcription of genes associated with butyrate production and boost production of butyrate *in vivo*. Enhanced production of butyrate is required for SAS-induced, microbe-dependent protection from experimental colitis in mice. Furthermore, SAS-enhanced production of butyrate was also seen in gnotobiotic mice colonized with responder microbiomes, and not non-responder microbiomes, suggesting the sufficiency of the microbiome to imprint this response. Additional colonization of non-responder microbiome-colonized mice with lead responder-marker taxa *F. prausnitzii* was sufficient to recover SAS protection against experimental colitis. Although our results do not exclude additional contributions of anti-inflammatory effectors produced by *F. prausnitzii*,[45] they do highlight the ability of SAS to promote the production of SCFA in an SP-dependent fashion and to promote protection against experimental colitis. Previous reports have defined a role for gut-derived butyrate in reducing inflammatory arthritis,[46,47] but the cellular effectors mediating systemic inflammation in IBD-pSpA still need to be defined. Collectively, these data highlight a functional interaction of SAS with specific bacterial taxa that offer the potential to not only stratify patients likely to respond to SAS therapy but also guide interventional microbial therapies to enhance the efficacy of SAS for IBD-SpA.

Folate plays a critical role in one carbon metabolism in multiple cellular reactions that are required to produce amino acids, thymidine, and purines.[48,49] The inhibition of bacterial *de novo* folate biosynthesis by SP moiety of SAS can therefore activate folate stress pathways.[26,37] *F. prausnitzii* encodes a *folP*-like enzyme called MBL-fold metallohydrolase, which is likely a target of SP.[36] Consistent with cellular sensing of *folP* inhibition, we observed upregulation in *folC* and *folT* following SP treatment of *F. prausnitzii.* Similarly highlighting the role for folate stress pathways, SP induction of butyrate synthesis genes was suppressed by excess folate. Other commensals, such as *E. rectale*, which do produce butyrate and encode *but*, do not regulate butyrate synthesis in response to SP. *E. rectale* does not encode *folP*, which may confer specificity of the SP effect on butyrate synthesis. Even though all patients in this study received folate supplementation, oral supplementation with folate is primarily absorbed in the small intestine, while SAS prodrug cleavage by microbial azoreductases to release SP and 5-ASA occurs distally in the colon.[39] Consistent with a functional antifolate effect of SP, evidence of a folate trap in the fecal metabolome of responders (but not non-responders) highlight the potential role for the microbiome in the clinical efficacy of SAS for pSpA. Recent work in *E. coli* revealed the ability of sub-inhibitory levels of the antifolate sulfamethoxazole in triggering antioxidant immunomodulatory metabolites called colipterins, further highlighting a potentially broader impact of folate regulation in host-microbe immunity.[26]

Studies of drug-host-microbe interactions are just beginning to elucidate how xenobiotics regulate microbial metabolic function and subsequently impact host immunity.[26,38] Our results highlight the potential role for microbial biomarkers in stratifying therapeutic responses to SAS, as well as the potential for microbial-based therapies in optimizing and enhancing medication efficacy. Management of IBD-pSpA remains an unmet need, and these findings have the potential to shape precision medicine to enhance therapeutic strategies.

Limitations of the study

The robust ability of *F. prausnitzii* and *R. callidus* combined to discriminate responders in a validation cohort highlights the potential clinical impact of these findings, but the limited sample size and the observational nature of our trial will require additional studies for prospective evaluation and assessment of demographic features including gender as a contributing factor. Additionally, the specificity and sensitivity of these markers in predicting SAS response compared to treatment with other biologic or small-molecule therapies for the treatment of IBD and pSpA still need to be investigated.

STAR★METHODS

Detailed methods are provided in the online version of this paper and include the following:

- KEY RESOURCES TABLE
- RESOURCE AVAILABILITY
  - Lead contact
  - Materials availability
  - Data and code availability
- EXPERIMENTAL MODEL AND STUDY PARTICIPANT DETAILS
  - Human samples
  - Mouse models
- METHOD DETAILS
  - Endpoint analysis
  - Fecal DNA extraction
  - Metagenomic analysis
  - Metabolomic analysis
  - 16S rRNA sequencing
  - *In vitro* assays and bacterial RNA-seq
  - Quantitative RT-PCR
- QUANTIFICATION AND STATISTICAL ANALYSIS

SUPPLEMENTAL INFORMATION

Supplemental information can be found online at https://doi.org/10.1016/j.xcrm.2024.101431.

ACKNOWLEDGMENTS

We would like to acknowledge members of the Longman Laboratory for helpful discussions regarding work performed for the manuscript. We would like to thank the Metabolomics, Genomics, and Microbiome Cores of Weill Cornell Medicine. This work was supported by grants from the NIDDK, R01 120985, R01 128257, and R01 DK114252 (to R.S.L.). Graphical abstract was created with BioRender (BioRender.com).

AUTHOR CONTRIBUTIONS

S.F.L., L.A.M., E.J.S., and R.S.L. conceived and designed this study; S.F.L., S.P., and R.S.L. designed the experiments; S.F.L., S.P., A.R., S.O., W.-B.J., G.F.-dP., G.M., M.V., W.Y., N.T., G.X., and R.S.L. performed experiments and analyzed the data; A.M., G.P., and A.G. performed bioinformatic analyses; C.-J.G., D.L., L.A.M., and E.J.S. provided critical reagents, technical advice, and material support; and S.F.L., S.P., and R.S.L. wrote the manuscript with input from all co-authors.

DECLARATION OF INTERESTS

The authors declare no competing interests.

Received: July 3, 2023
Revised: November 28, 2023
Accepted: January 25, 2024
Published: February 19, 2024

REFERENCES

1. Ossum, A.M., Palm, Ø., Lunder, A.K., Cvancarova, M., Banitalebi, H., Negård, A., Høie, O., Henriksen, M., Moum, B.A., and Høivik, M.L.; IBSEN Study Group (2018). Ankylosing Spondylitis and Axial Spondyloarthritis in Patients With Long-term Inflammatory Bowel Disease: Results From 20 Years of Follow-up in the IBSEN Study. J. Crohns Colitis *12*, 96–104, PubMed PMID: 28961700. https://doi.org/10.1093/ecco-jcc/jjx126.
2. van Erp, S.J., Brakenhoff, L.K., van Gaalen, F.A., van den Berg, R., Fidder, H.H., Verspaget, H.W., Huizinga, T.W., Veenendaal, R.A., Wolterbeek, R., van der Heijde, D., et al. (2016). Classifying Back Pain and Peripheral Joint Complaints in Inflammatory Bowel Disease Patients: A Prospective Longitudinal Follow-up Study. J. Crohns Colitis *10*, 166–175, PubMed PMID: 26512134. https://doi.org/10.1093/ecco-jcc/jjv195.
3. Palm, Ø., Moum, B., Jahnsen, J., and Gran, J.T. (2001). The prevalence and incidence of peripheral arthritis in patients with inflammatory bowel disease, a prospective population-based study (the IBSEN study). Rheumatology *40*, 1256–1261, PubMed PMID: 11709609. https://doi.org/10.1093/rheumatology/40.11.1256.
4. Orchard, T.R., Wordsworth, B.P., and Jewell, D.P. (1998). Peripheral arthropathies in inflammatory bowel disease: their articular distribution and natural history. Gut *42*, 387–391, PubMed PMID: 9577346; PMCID: PMC1727027. https://doi.org/10.1136/gut.42.3.387.
5. Ditisheim, S., Fournier, N., Juillerat, P., Pittet, V., Michetti, P., Gabay, C., and Finckh, A.; Swiss IBD Cohort Study Group (2015). Inflammatory Articular Disease in Patients with Inflammatory Bowel Disease: Result of the Swiss IBD Cohort Study. Inflamm. Bowel Dis. *21*, 2598–2604, PubMed PMID: 26244648. https://doi.org/10.1097/MIB.0000000000000548.
6. Karreman, M.C., Luime, J.J., Hazes, J.M.W., and Weel, A.E.A.M. (2017). The Prevalence and Incidence of Axial and Peripheral Spondyloarthritis in Inflammatory Bowel Disease: A Systematic Review and Meta-analysis. J. Crohns Colitis *11*, 631–642, PubMed PMID: 28453761. https://doi.org/10.1093/ecco-jcc/jjw199.
7. Harbord, M., Annese, V., Vavricka, S.R., Allez, M., Barreiro-de Acosta, M., Boberg, K.M., Burisch, J., De Vos, M., De Vries, A.M., Dick, A.D., et al. (2016). The First European Evidence-based Consensus on Extra-intestinal Manifestations in Inflammatory Bowel Disease. J. Crohns Colitis *10*, 239–254, PubMed PMID: 26614685; PMCID: PMC4957476. https://doi.org/10.1093/ecco-jcc/jjv213.
8. Kumar, A., Lukin, D., Battat, R., Schwartzman, M., Mandl, L.A., Scherl, E., and Longman, R.S. (2020). Defining the phenotype, pathogenesis and treatment of Crohn's disease associated spondyloarthritis. J. Gastroenterol. *55*, 667–678, PubMed PMID: 32367294; PMCID: PMC7297835. https://doi.org/10.1007/s00535-020-01692-w.
9. Tito, R.Y., Cypers, H., Joossens, M., Varkas, G., Van Praet, L., Glorieus, E., Van den Bosch, F., De Vos, M., Raes, J., and Elewaut, D. (2017). Brief Report: Dialister as a Microbial Marker of Disease Activity in Spondyloarthritis. Arthritis Rheumatol. *69*, 114–121, PubMed PMID: 27390077. https://doi.org/10.1002/art.39802.
10. Muñiz Pedrogo, D.A., Chen, J., Hillmann, B., Jeraldo, P., Al-Ghalith, G., Taneja, V., Davis, J.M., Knights, D., Nelson, H., Faubion, W.A., et al. (2019). An Increased Abundance of Clostridiaceae Characterizes Arthritis in Inflammatory Bowel Disease and Rheumatoid Arthritis: A Cross-sectional Study. Inflamm. Bowel Dis. *25*, 902–913, PubMed PMID: 30321331; PMCID: PMC6458525. https://doi.org/10.1093/ibd/izy318.
11. Breban, M., Tap, J., Leboime, A., Said-Nahal, R., Langella, P., Chiocchia, G., Furet, J.P., and Sokol, H. (2017). Faecal microbiota study reveals specific dysbiosis in spondyloarthritis. Ann. Rheum. Dis. *76*, 1614–1622, PubMed PMID: 28606969. https://doi.org/10.1136/annrheumdis-2016-211064.
12. Viladomiu, M., Kivolowitz, C., Abdulhamid, A., Dogan, B., Victorio, D., Castellanos, J.G., Woo, V., Teng, F., Tran, N.L., Sczesnak, A., et al. (2017). IgA-coated E. coli enriched in Crohn's disease spondyloarthritis promote TH17-dependent inflammation. Sci. Transl. Med. *9*, eaaf9655, PubMed PMID: 28179509. https://doi.org/10.1126/scitranslmed.aaf9655.
13. Viladomiu, M., Metz, M.L., Lima, S.F., Jin, W.B., Chou, L., Bank, J.R.I.L.C., Guo, C.J., Diehl, G.E., Simpson, K.W., Scherl, E.J., and Longman, R.S. (2021). Adherent-invasive E. coli metabolism of propanediol in Crohn's disease regulates phagocytes to drive intestinal inflammation. Cell Host Microbe *29*, 607–619.e8, PubMed PMID: 33539767; PMCID: PMC8049981. https://doi.org/10.1016/j.chom.2021.01.002.
14. Berland, M., Meslier, V., Berreira Ibraim, S., Le Chatelier, E., Pons, N., Maziers, N., Thirion, F., Gauthier, F., Plaza Onate, F., Furet, J.P., et al. (2023). Both Disease Activity and HLA-B27 Status Are Associated With Gut Microbiome Dysbiosis in Spondyloarthritis Patients. Arthritis Rheumatol. *75*, 41–52, PubMed PMID: 35818337; PMCID: PMC10099252. https://doi.org/10.1002/art.42289.
15. Misiewicz, J.J., Lennard-Jones, J.E., Connell, A.M., Baron, J.H., and Avery Jones, F. (1965). Controlled trial of sulphasalazine in maintenance therapy for ulcerative colitis. Lancet *285*, 185–188. https://doi.org/10.1016/S0140-6736(65)90972-4.
16. Baron, J.H., Connell, A.M., Lennard-Jones, J.E., and Jones, F.A. (1962). Sulphasalazine and salicylazosulphadimidine in ulcerative colitis. Lancet *1*, 1094–1096, PubMed PMID: 13865153. https://doi.org/10.1016/s0140-6736(62)92080-9.
17. Dick, A.P., Grayson, M.J., Carpenter, R.G., and Petrie, A. (1964). Controlled Trial of Sulphasalazine in the Treatment of Ulcerative Colitis. Gut *5*, 437–442, PubMed PMID: 14218553; PMCID: PMC1552152. https://doi.org/10.1136/gut.5.5.437.
18. Dissanayake, A.S., and Truelove, S.C. (1973). Proceedings: A controlled therapeutic trial of long-term maintenance treatment of ulcerative colitis with sulphasalazine (salazopyrin). Gut *14*, 818. PubMed PMID: 4148469.
19. Svartz, M. (1948). The treatment of 124 cases of ulcerative colitis with salazopyrine and attempts of desensibilization in cases of hypersensitiveness to sulfa. Acta Med. Scand. *131* (*Suppl 206*), 465–472, PubMed PMID: 18881171. https://doi.org/10.1111/j.0954-6820.1948.tb12083.x.
20. Peppercorn, M.A., and Goldman, P. (1972). The role of intestinal bacteria in the metabolism of salicylazosulfapyridine. J. Pharmacol. Exp. Ther. *181*, 555–562. PubMed PMID: 4402374.
21. Byndloss, M.X., Olsan, E.E., Rivera-Chavez, F., Tiffany, C.R., Cevallos, S.A., Lokken, K.L., Torres, T.P., Byndloss, A.J., Faber, F., Gao, Y., et al.

(2017). Microbiota-activated PPAR-gamma signaling inhibits dysbiotic Enterobacteriaceae expansion. Science *357*, 570–575, PubMed PMID: 28798125; PMCID: PMC5642957. https://doi.org/10.1126/science.aam9949.

22. Azad Khan, A.K., Piris, J., and Truelove, S.C. (1977). An experiment to determine the active therapeutic moiety of sulphasalazine. Lancet *2*, 892–895, PubMed PMID: 72239. https://doi.org/10.1016/s0140-6736(77)90831-5.

23. Clegg, D.O., Reda, D.J., and Abdellatif, M. (1999). Comparison of sulfasalazine and placebo for the treatment of axial and peripheral articular manifestations of the seronegative spondylarthropathies: a Department of Veterans Affairs cooperative study. Arthritis Rheum. *42*, 2325–2329, PubMed PMID: 10555027. https://doi.org/10.1002/1529-0131(199911)42:11<2325::AID-ANR10>3.0.CO;2-C.

24. Kanerud, L., Scheynius, A., Nord, C.E., and Hafström, I. (1994). Effect of sulphasalazine on gastrointestinal microflora and on mucosal heat shock protein expression in patients with rheumatoid arthritis. Br. J. Rheumatol. *33*, 1039–1048, PubMed PMID: 7981991. https://doi.org/10.1093/rheumatology/33.11.1039.

25. Zheng, H., Chen, M., Li, Y., Wang, Y., Wei, L., Liao, Z., Wang, M., Ma, F., Liao, Q., and Xie, Z. (2017). Modulation of Gut Microbiome Composition and Function in Experimental Colitis Treated with Sulfasalazine. Front. Microbiol. *8*, 1703, PubMed PMID: 28936203; PMCID: PMC5594074. https://doi.org/10.3389/fmicb.2017.01703.

26. Park, H.B., Wei, Z., Oh, J., Xu, H., Kim, C.S., Wang, R., Wyche, T.P., Piizzi, G., Flavell, R.A., and Crawford, J.M. (2020). Sulfamethoxazole drug stress upregulates antioxidant immunomodulatory metabolites in Escherichia coli. Nat. Microbiol. *5*, 1319–1329, PubMed PMID: 32719505; PMCID: PMC7581551. https://doi.org/10.1038/s41564-020-0763-4.

27. van der Heijde, D., Sieper, J., Maksymowych, W.P., Dougados, M., Burgos-Vargas, R., Landewé, R., Rudwaleit, M., and Braun, J.; Assessment of SpondyloArthritis international Society (2011). 2010 Update of the international ASAS recommendations for the use of anti-TNF agents in patients with axial spondyloarthritis. Ann. Rheum. Dis. *70*, 905–908, PubMed PMID: 21540200. https://doi.org/10.1136/ard.2011.151563.

28. Garrett, S., Jenkinson, T., Kennedy, L.G., Whitelock, H., Gaisford, P., and Calin, A. (1994). A new approach to defining disease status in ankylosing spondylitis: the Bath Ankylosing Spondylitis Disease Activity Index. J. Rheumatol. *21*, 2286–2291. PubMed PMID: 7699630.

29. Lai, D., Funez-Depagnier, G., Duenas-Bianchi, L., Lavergne, A., Battat, R., Ahmed, W., Schwartzman, M., Lima, S., Khan, S., Chong, P.S., et al. (2022). Joint Disease Activity in Inflammatory Bowel Disease-associated Peripheral Spondyloarthritis Stratifies Therapeutic Response. Gastro Hep Adv *1*, 137–140, PubMed PMID: 35441160; PMCID: PMC9015680. https://doi.org/10.1016/j.gastha.2021.12.002.

30. Lukas, C., Landewé, R., Sieper, J., Dougados, M., Davis, J., Braun, J., van der Linden, S., and van der Heijde, D.; Assessment of SpondyloArthritis international Society (2009). Assessment of SpondyloArthritis international S. Development of an ASAS-endorsed disease activity score (ASDAS) in patients with ankylosing spondylitis. Ann. Rheum. Dis. *68*, 18–24, PubMed PMID: 18625618. https://doi.org/10.1136/ard.2008.094870.

31. Segata, N., Izard, J., Waldron, L., Gevers, D., Miropolsky, L., Garrett, W.S., and Huttenhower, C. (2011). Metagenomic biomarker discovery and explanation. Genome Biol. *12*, R60, PubMed PMID: 21702898; PMCID: PMC3218848. https://doi.org/10.1186/gb-2011-12-6-r60.

32. Morgan, X.C., Tickle, T.L., Sokol, H., Gevers, D., Devaney, K.L., Ward, D.V., Reyes, J.A., Shah, S.A., LeLeiko, N., Snapper, S.B., et al. (2012). Dysfunction of the intestinal microbiome in inflammatory bowel disease and treatment. Genome Biol. *13*, R79, PubMed PMID: 23013615; PMCID: PMC3506950. https://doi.org/10.1186/gb-2012-13-9-r79.

33. Rao, K.S., Albro, M., Dwyer, T.M., and Frerman, F.E. (2006). Kinetic mechanism of glutaryl-CoA dehydrogenase. Biochemistry *45*, 15853–15861, PubMed PMID: 17176108. https://doi.org/10.1021/bi0609016.

34. Erb, T.J., Brecht, V., Fuchs, G., Muller, M., and Alber, B.E. (2009). Carboxylation mechanism and stereochemistry of crotonyl-CoA carboxylase/reductase, a carboxylating enoyl-thioester reductase. Proc Natl Acad Sci USA *106*, 8871–8876, PubMed PMID: 19458256; PMCID: PMC2689996. https://doi.org/10.1073/pnas.0903939106.

35. Klotz, U. (1985). Clinical pharmacokinetics of sulphasalazine, its metabolites and other prodrugs of 5-aminosalicylic acid. Clin. Pharmacokinet. *10*, 285–302, PubMed PMID: 2864155. https://doi.org/10.2165/00003088-198510040-00001.

36. Xu, H., Aurora, R., Rose, G.D., and White, R.H. (1999). Identifying two ancient enzymes in Archaea using predicted secondary structure alignment. Nat. Struct. Biol. *6*, 750–754, PubMed PMID: 10426953. https://doi.org/10.1038/11525.

37. Guzzo, M.B., Nguyen, H.T., Pham, T.H., Wyszczelska-Rokiel, M., Jakubowski, H., Wolff, K.A., Ogwang, S., Timpona, J.L., Gogula, S., Jacobs, M.R., et al. (2016). Methylfolate Trap Promotes Bacterial Thymineless Death by Sulfa Drugs. PLoS Pathog. *12*, e1005949, PubMed PMID: 27760199; PMCID: PMC5070874. https://doi.org/10.1371/journal.ppat.1005949.

38. Nayak, R.R., Alexander, M., Deshpande, I., Stapleton-Gray, K., Rimal, B., Patterson, A.D., Ubeda, C., Scher, J.U., and Turnbaugh, P.J. (2021). Methotrexate impacts conserved pathways in diverse human gut bacteria leading to decreased host immune activation. Cell Host Microbe *29*, 362–377.e11, PubMed PMID: 33440172; PMCID: PMC7954989. https://doi.org/10.1016/j.chom.2020.12.008.

39. Svartz, N. (1942). Salazopyrin, a new sulfanilamide preparation. A. Therapeutic Results in Rheumatic Polyarthritis. B. Therapeutic Results in Ulcerative Colitis. C. Toxic Manifestations in Treatment with Sulfanilamide Preparations. Acta Med. Scand. https://doi.org/10.1111/j.0954-6820.1942.tb06841.x.

40. Walter, J., Armet, A.M., Finlay, B.B., and Shanahan, F. (2020). Establishing or Exaggerating Causality for the Gut Microbiome: Lessons from Human Microbiota-Associated Rodents. Cell *180*, 221–232, PubMed PMID: 31978342. https://doi.org/10.1016/j.cell.2019.12.025.

41. Sokol, H., Pigneur, B., Watterlot, L., Lakhdari, O., Bermúdez-Humarán, L.G., Gratadoux, J.J., Blugeon, S., Bridonneau, C., Furet, J.P., Corthier, G., et al. (2008). Faecalibacterium prausnitzii is an anti-inflammatory commensal bacterium identified by gut microbiota analysis of Crohn disease patients. Proc. Natl. Acad. Sci. USA *105*, 16731–16736. Epub 2008/10/22. doi: 0804812105 [pii]10.1073/pnas.0804812105. PubMed PMID: 18936492; PMCID: 2575488.

42. Atarashi, K., Tanoue, T., Shima, T., Imaoka, A., Kuwahara, T., Momose, Y., Cheng, G., Yamasaki, S., Saito, T., Ohba, Y., et al. (2011). Ivanov II, Umesaki Y, Itoh K, Honda K. Induction of colonic regulatory T cells by indigenous Clostridium species. Science *331*, 337–341, PubMed PMID: 21205640; PMCID: PMC3969237. https://doi.org/10.1126/science.1198469.

43. Furusawa, Y., Obata, Y., Fukuda, S., Endo, T.A., Nakato, G., Takahashi, D., Nakanishi, Y., Uetake, C., Kato, K., Kato, T., et al. (2013). Commensal microbe-derived butyrate induces the differentiation of colonic regulatory T cells. Nature *504*, 446–450, PubMed PMID: 24226770. https://doi.org/10.1038/nature12721.

44. Mehta, R.S., Mayers, J.R., Zhang, Y., Bhosle, A., Glasser, N.R., Nguyen, L.H., Ma, W., Bae, S., Branck, T., Song, K., et al. (2023). Gut microbial metabolism of 5-ASA diminishes its clinical efficacy in inflammatory bowel disease. Nat. Med. *29*, 700–709, PubMed PMID: 36823301. https://doi.org/10.1038/s41591-023-02217-7.

45. Quévrain, E., Maubert, M.A., Michon, C., Chain, F., Marquant, R., Tailhades, J., Miquel, S., Carlier, L., Bermúdez-Humarán, L.G., Pigneur, B., et al. (2016). Identification of an anti-inflammatory protein from Faecalibacterium prausnitzii, a commensal bacterium deficient in Crohn's disease. Gut *65*, 415–425, PubMed PMID: 26045134; PMCID: PMC5136800. https://doi.org/10.1136/gutjnl-2014-307649.

46. Rosser, E.C., Piper, C.J.M., Matei, D.E., Blair, P.A., Rendeiro, A.F., Orford, M., Alber, D.G., Krausgruber, T., Catalan, D., Klein, N., et al. (2020). Microbiota-Derived Metabolites Suppress Arthritis by Amplifying Aryl-Hydrocarbon

Receptor Activation in Regulatory B Cells. Cell Metab *31*, 837–851.e10, PubMed PMID: 32213346; PMCID: PMC7156916. https://doi.org/10.1016/j.cmet.2020.03.003.

47. Hui, W., Yu, D., Cao, Z., and Zhao, X. (2019). Butyrate inhibit collagen-induced arthritis via Treg/IL-10/Th17 axis. Int. Immunopharmacol. *68*, 226–233, PubMed PMID: 30660077. https://doi.org/10.1016/j.intimp.2019.01.018.
48. Ducker, G.S., and Rabinowitz, J.D. (2017). One-Carbon Metabolism in Health and Disease. Cell Metab. *25*, 27–42, PubMed PMID: 27641100; PMCID: PMC5353360. https://doi.org/10.1016/j.cmet.2016.08.009.
49. Selhub, J. (2002). Folate, vitamin B12 and vitamin B6 and one carbon metabolism. J. Nutr. Health Aging *6*, 39–42. PubMed PMID: 11813080.
50. Lima, S.F., Gogokhia, L., Viladomiu, M., Chou, L., Putzel, G., Jin, W.B., Pires, S., Guo, C.J., Gerardin, Y., Crawford, C.V., et al. (2022). Transferable Immunoglobulin A-Coated Odoribacter splanchnicus in Responders to Fecal Microbiota Transplantation for Ulcerative Colitis Limits Colonic Inflammation. Gastroenterology *162*, 166–178, PubMed PMID: 34606847; PMCID: PMC8678328. https://doi.org/10.1053/j.gastro.2021.09.061.
51. Walters, W., Hyde, E.R., Berg-Lyons, D., Ackermann, G., Humphrey, G., Parada, A., Gilbert, J.A., Jansson, J.K., Caporaso, J.G., Fuhrman, J.A., et al. (2016). Improved Bacterial 16S rRNA Gene (V4 and V4-5) and Fungal Internal Transcribed Spacer Marker Gene Primers for Microbial Community Surveys. mSystems *1*, PubMed PMID: 27822518; PMCID: PMC5069754. https://doi.org/10.1128/mSystems.00009-15.
52. Rudwaleit, M., van der Heijde, D., Landewé, R., Akkoc, N., Brandt, J., Chou, C.T., Dougados, M., Huang, F., Gu, J., Kirazli, Y., et al. (2011). The Assessment of SpondyloArthritis International Society classification criteria for peripheral spondyloarthritis and for spondyloarthritis in general. Ann. Rheum. Dis. *70*, 25–31, PubMed PMID: 21109520. https://doi.org/10.1136/ard.2010.133645.
53. Machado, P.M.M.C., Landewé, R.B.M., and van der Heijde, D.M. (2011). Endorsement of definitions of disease activity states and improvement scores for the Ankylosing Spondylitis Disease Activity Score: results from OMERACT 10. J. Rheumatol. *38*, 1502–1506, PubMed PMID: 21724723. https://doi.org/10.3899/jrheum.110279.
54. Park, S.H., Choe, J.Y., Kim, S.K., Lee, H., Castrejón, I., and Pincus, T. (2015). Routine Assessment of Patient Index Data (RAPID3) and Bath Ankylosing Spondylitis Disease Activity Index (BASDAI) Scores Yield Similar Information in 85 Korean Patients With Ankylosing Spondylitis Seen in Usual Clinical Care. J. Clin. Rheumatol. *21*, 300–304, PubMed PMID: 26308349; PMCID: PMC4629489. https://doi.org/10.1097/RHU.0000000000000277.
55. Turnbaugh, P.J., Ridaura, V.K., Faith, J.J., Rey, F.E., Knight, R., and Gordon, J.I. (2009). The effect of diet on the human gut microbiome: a metagenomic analysis in humanized gnotobiotic mice. Sci. Transl. Med. *1*, 6ra14, PubMed PMID: 20368178; PMCID: PMC2894525. https://doi.org/10.1126/scitranslmed.3000322.
56. Vermeire, S., Schreiber, S., Sandborn, W.J., Dubois, C., and Rutgeerts, P. (2010). Correlation between the Crohn's disease activity and Harvey-Bradshaw indices in assessing Crohn's disease severity. Clin. Gastroenterol. Hepatol. *8*, 357–363, PubMed PMID: 20096379. https://doi.org/10.1016/j.cgh.2010.01.001.
57. Bolger, A.M., Lohse, M., and Usadel, B. (2014). Trimmomatic: a flexible trimmer for Illumina sequence data. Bioinformatics *30*, 2114–2120, PubMed PMID: 24695404; PMCID: PMC4103590. https://doi.org/10.1093/bioinformatics/btu170.
58. Truong, D.T., Franzosa, E.A., Tickle, T.L., Scholz, M., Weingart, G., Pasolli, E., Tett, A., Huttenhower, C., and Segata, N. (2015). MetaPhlAn2 for enhanced metagenomic taxonomic profiling. Nat. Methods *12*, 902–903, PubMed PMID: 26418763. https://doi.org/10.1038/nmeth.3589.
59. Langmead, B., and Salzberg, S.L. (2012). Fast gapped-read alignment with Bowtie 2. Nat. Methods *9*, 357–359, PubMed PMID: 22388286; PMCID: PMC3322381. https://doi.org/10.1038/nmeth.1923.
60. Abubucker, S., Segata, N., Goll, J., Schubert, A.M., Izard, J., Cantarel, B.L., Rodriguez-Mueller, B., Zucker, J., Thiagarajan, M., Henrissat, B., et al. (2012). Metabolic reconstruction for metagenomic data and its application to the human microbiome. PLoS Comput. Biol. *8*, e1002358, PubMed PMID: 22719234; PMCID: PMC3374609. https://doi.org/10.1371/journal.pcbi.1002358.
61. Buchfink, B., Xie, C., and Huson, D.H. (2015). Fast and sensitive protein alignment using DIAMOND. Nat. Methods *12*, 59–60, PubMed PMID: 25402007. https://doi.org/10.1038/nmeth.3176.
62. Suzek, B.E., Wang, Y., Huang, H., McGarvey, P.B., and Wu, C.H.; UniProt Consortium (2015). UniRef clusters: a comprehensive and scalable alternative for improving sequence similarity searches. Bioinformatics *31*, 926–932, PubMed PMID: 25398609; PMCID: PMC4375400. https://doi.org/10.1093/bioinformatics/btu739.
63. Caspi, R., Billington, R., Fulcher, C.A., Keseler, I.M., Kothari, A., Krummenacker, M., Latendresse, M., Midford, P.E., Ong, Q., Ong, W.K., et al. (2018). The MetaCyc database of metabolic pathways and enzymes. Nucleic Acids Res. *46*, D633–D639, PubMed PMID: 29059334; PMCID: PMC5753197. https://doi.org/10.1093/nar/gkx935.
64. Lu, Y., Yao, D., and Chen, C. (2013). 2-Hydrazinoquinoline as a Derivatization Agent for LC-MS-Based Metabolomic Investigation of Diabetic Ketoacidosis. Metabolites *3*, 993–1010, PubMed PMID: 24958262; PMCID: PMC3937830. https://doi.org/10.3390/metabo3040993.
65. Callahan, B.J., McMurdie, P.J., Rosen, M.J., Han, A.W., Johnson, A.J.A., and Holmes, S.P. (2016). DADA2: High-resolution sample inference from Illumina amplicon data. Nat. Methods *13*, 581–583, PubMed PMID: 27214047; PMCID: PMC4927377. https://doi.org/10.1038/nmeth.3869.
66. Rognes, T., Flouri, T., Nichols, B., Quince, C., and Mahe, F. (2016). VSEARCH: a versatile open source tool for metagenomics. PeerJ *4*, e2584, PubMed PMID: 27781170; PMCID: PMC5075697.. https://doi.org/10.7717/peerj.2584
67. Quast, C., Pruesse, E., Yilmaz, P., Gerken, J., Schweer, T., Yarza, P., Peplies, J., and Glöckner, F.O. (2013). The SILVA ribosomal RNA gene database project: improved data processing and web-based toolsDatabase issue. Nucleic Acids Res. *41*, D590–D596, PubMed PMID: 23193283; PMCID: PMC3531112. https://doi.org/10.1093/nar/gks1219.
68. McMurdie, P.J., and Holmes, S. (2013). phyloseq: an R package for reproducible interactive analysis and graphics of microbiome census data. PLoS One *8*, e61217, PubMed PMID: 23630581; PMCID: PMC3632530. https://doi.org/10.1371/journal.pone.0061217.
69. Dobin, A., Davis, C.A., Schlesinger, F., Drenkow, J., Zaleski, C., Jha, S., Batut, P., Chaisson, M., and Gingeras, T.R. (2013). STAR: ultrafast universal RNA-seq aligner. Bioinformatics *29*, 15–21, PubMed PMID: 23104V. https://doi.org/10.1093/bioinformatics/bts635.
70. Hartley, S.W., and Mullikin, J.C. (2015). QoRTs: a comprehensive toolset for quality control and data processing of RNA-Seq experiments. BMC Bioinf. *16*, 224, PubMed PMID: 26187896; PMCID: PMC4506620. https://doi.org/10.1186/s12859-015-0670-5.
71. Liao, Y., Smyth, G.K., and Shi, W. (2014). featureCounts: an efficient general purpose program for assigning sequence reads to genomic features. Bioinformatics *30*, 923–930, PubMed PMID: 24227677. https://doi.org/10.1093/bioinformatics/btt656.
72. Karp, P.D., Billington, R., Caspi, R., Fulcher, C.A., Latendresse, M., Kothari, A., Keseler, I.M., Krummenacker, M., Midford, P.E., Ong, Q., et al. (2019). The BioCyc collection of microbial genomes and metabolic pathways. Brief. Bioinform. *20*, 1085–1093, PubMed PMID: 29447345; PMCID: PMC6781571. https://doi.org/10.1093/bib/bbx085.
73. Love, M.I., Huber, W., and Anders, S. (2014). Moderated estimation of fold change and dispersion for RNA-seq data with DESeq2. Genome Biol. *15*, 550, PubMed PMID: 25516281; PMCID: PMC4302049. https://doi.org/10.1186/s13059-014-0550-8.

STAR★METHODS

KEY RESOURCES TABLE

REAGENT or RESOURCE	SOURCE	IDENTIFIER
Bacterial and virus strains		
F. prausnitzii	ATCC	27768
E. rectale	DSM	17629
Biological samples		
Human fecal samples	This study	N/A
Chemicals, peptides, and recombinant proteins		
Sodium hydroxide (NaOH)	Sigma-Aldrich	Cat# 1310-73-2
Sulfapyridine	Sigma-Aldrich	Cat# 144-83-2
Sulfasalazine	Sigma-Aldrich	Cat# 599-79-1
Balsalazide	TCI	Cat# 150399-21-6
Dextran Sodium Sulfate	Affymetrix	Cat# 9011-18-1
YCFAC Media	Anaerobe Systems	Cat# AS-675
RCM Media	BD Difco	Cat# DF1808-17-3
Folate	Sigma-Aldrich	Cat# 59-30-3
Critical commercial assays		
Mouse Lipocalin-2/NGAL DuoSet ELISA	R&D Systems	Cat# DY1857
RNeasy PowerMicrobiome kit	QIAGEN	Cat# 26000-50
RNeasy Plus Mini Kit	QIAGEN	Cat# 74134
RNeasy Plus Micro Kit	QIAGEN	Cat# 74034
qScript cDNA SuperMix kit	Quantabio, Beverly, MA	Cat# 95048
PerfeCTa SYBR Green Fast mix, Low ROX	Quantabio, Beverly, MA	Cat# 95074
DNeasy PowerLyzer PowerSoil Kit	Qiagen	Cat# 12855
iScript cDNA synthesis kit	Bio-Rad	Cat# 1708891
Deposited data		
Human microbiome sequencing data	NCBI SRA	BioProject ID PRJNA929558
Mouse microbiome sequencing data	NCBI SRA	BioProject ID PRJNA930470
Bacterial *in vitro* sequencing data	NCBI SRA	BioProject ID PRJNA930465
Experimental models: Organisms/strains		
Mouse: C57BL/6	Jackson Laboratories	Cat# 000664
Mouse: Gpr109a−/−	Lima et al.[50]	N/A
Oligonucleotides		
16S rRNA gene −515F 5′ GTGYCAGCMGCCGCGGTAA 3′, −926R 5′ CCGYCAATTYMTTTRAGTTT 3′	Walters et al.[51]	N/A
F. prausnitzii but gene F: 5′ GTGGATGCCTTTGTGGATATTG 3′, R: 5′ CCGGGTTATCGTTCAGGTAATC 3′	This work	N/A
E. rectale but gene F: 5′ CTCAGCAGATGAGGCAGTAAAG 3′, R: 5′ GGAAGCTCTGAGTAACGGATTG 3′	This work	N/A
Software and algorithms		
R	R Core Team	N/A
GraphPad Prism 7	GraphPad Software	N/A
JMP 14	SAS Institute Inc., Cary, NC	N/A

RESOURCE AVAILABILITY

Lead contact

Further information and requests for resources and reagents should be directed to and will be fulfilled by lead contact, Randy Longman (ral2006@med.cornell.edu).

Materials availability

This study did not generate new unique reagents.

Data and code availability

(1) Fastq files from human, mouse and bacterial *in vitro* experiments are available in NCBI's Sequence Read Archive, BioProject ID PRJNA929558, PRJNA930470, and PRJNA930465, respectively.
(2) This paper does not report original code.
(3) Any additional information required to reanalyze the data reported in this paper is available from the lead contact upon request.

EXPERIMENTAL MODEL AND STUDY PARTICIPANT DETAILS

Human samples

Sequential subjects with clinical diagnoses of both IBD and ASAS-defined pSpA and an indication for treatment with SAS were prospectively evaluated and longitudinally followed at the Jill Roberts Center for Inflammatory Bowel Disease at Weill Cornell Medicine (WCM, Supplementary Table S1) between December 2015 and March 2020. Eligible patients of any gender were between the ages of 18–80 with ulcerative colitis (UC) or Crohn's disease (CD) and ASAS criteria of pSpA defined as the presence of peripheral arthritis, enthesitis or dactylitis.[52] Patients with active SpA, defined as ASDAS >1.3 and/or BASDAI $\geq$4, were eligible to participate.[53,54] Health status exclusion criteria included antibiotic use within 8 weeks prior enrollment, SAS use within 8 months prior enrollment, current pregnancy or lactation, an existing rheumatic disease to which the inflammatory-type joint symptoms were attributed (i.e., systemic lupus erythematosus, rheumatoid arthritis), or an ostomy. Participants who declined therapy or were intolerant of SAS were followed as standard of care controls. SAS subjects were prescribed 2g increasing to 4g of SAS daily as tolerated, and 1mg/day of folic acid. All patients provided voluntary informed consent and the study ethics was approved by the Weill Cornell institutional review board (IRB 1504016115).

A validation cohort of IBD SpA patients was selected from an ongoing biobank study of adult patients with IBD (IRB 1806019340). Exclusion criteria included antibiotic use, an existing rheumatic disease to which the inflammatory-type joint symptoms were attributed (i.e., systemic lupus erythematosus, rheumatoid arthritis), or an ostomy. From a total 442 subjects, we identified 16 subjects with IBD and SpA with sulfasalazine listed as a current medication. 5 subjects had active SpA symptoms and were characterized as non-responders, while 11 subjects had inactive SpA symptoms and characterized as responders. Fecal samples were analyzed by 16S rRNA analysis as described below.

Mouse models

Gnotobiotic C57BL/6 wild-type (WT) mice were bred and maintained at WCM Gnotobiotic Mouse facility. Specific pathogen free (SPF) C57BL/6 WT mice were ordered from Jackson Laboratory. C57BL/6 *Gpr109a*$^{-/-}$ mice were obtained from Marcel van den Brink laboratory and were bred and maintained under SPF conditions at WCM.

For induction of chemical colitis, 2% dextran sodium sulfate (DSS) (w/v) (M.W. 40,000–50,000; Affymetrix, Santa Clara, CA) was added to drinking water and administered *ad libitum* for 7 days. Mice were then monitored daily for weight loss and survival. Mouse Lipocalin-2 was measured in the cecal content supernatant using sandwich enzyme-linked immunosorbent assay (R&D Systems, Minneapolis, MN). Mice were treated with 300 mg/kg/day of SAS (Sigma-Aldrich, St. Louis, MO), balsalazide (BSD; TCI, America) or water vehicle control, as previously described.[25]

For gnotobiotic experiments, germ-free (GF) mice were gavaged with 1g of homogenized patient fecal samples diluted in 10mL of reduced PBS under anaerobic conditions, as previously described.[55] Mice gavaged with ATCC 27768 *F prausnitzii* received 1x10^{9} colony forming units (CFU) grown under anaerobic conditions at log-phase in Yeast Casitone Fatty Acids Broth with Carbohydrate media (YCFAC, Anaerobe Systems, Morgan Hill, CA).

All animal experiments were performed with 6-8-week-old WT, *Gpr109a*$^{-/-}$ and heterozygous littermate mice. Both female and male mice were used with random and equal assignment to each experimental group. All animal studies were carried out in accordance with protocols approved by the Institutional Animal Care and Use Committee at WCM.

METHOD DETAILS

Endpoint analysis

The primary endpoint of our analysis was clinical response in BASDAI, defined conservatively as a reduction in BASDAI of >2. Secondary endpoints were clinical response in ASDAS and Harvey-Bradshaw Index (HBI) for CD defined as reduction in ASDAS of $\geq$1.1 at week 12 post-study initiation[53] or a decrease in HBI of $\geq$3,[56] respectively. Exploratory analysis included absolute reduction in BASDAI, ASDAS, CRP, and HBI.

Fecal DNA extraction

Upon collection, stool samples were promptly divided into 2 mL aliquots and stored at −80°C. For microbiome analysis, DNA was isolated from approximately 250 mg of stool samples using the DNeasy PowerLyzer PowerSoil Kit (Qiagen, Hilden, Germany), following manufacturer's instructions.

Metagenomic analysis

To evaluate the impact of SAS on the fecal microbiome composition and its functional potential, we performed metagenomic sequencing. Metagenomic library was constructed with Illumina barcodes from the Nextera XT kit (Illumina, San Diego, CA) and then loaded into Illumina Hiseq 4000 platform using 2 x 150 nucleotide pair-ending sequencing protocol at Weill Cornell Microbiome Core. Sequencing data analysis is detailed in supplemental methods. Raw data was processed by KneadData (https://bitbucket.org/biobakery/kneaddata) to remove human contaminant reads. To filter out low quality sequence reads, sequences shorter than 50 bp and Illumina adapters reads, Trimmomatic[57] was used. Samples from three patients failed metagenomic library processing (BASDAI responders n = 2, BASDAI non-responders n = 1). After quality control, samples averaged 4 million reads (mean = 4,286,719.1, standard error of the mean - SEM ±251,131.1). Taxonomic profiling was determined by MetaPhlAn2 pipeline.[58] Microbial abundances were calculated with MetaPhlAn2, following Bowtie2[59] alignment to the MetaPhlAn2 database. Microbial functional potential profiling was determined by HUMAnN2.[60] For gene profiling, DIAMOND[61] was used to map metagenome reads against UniRef90.[62] Hits were counted for each gene family and normalized for length and alignment quality. For pathway profiling, gene family abundances were combined into structured pathways from MetaCyc[63] and then sum-normalized to copies per million (CPM).

Metabolomic analysis

To determine drug fecal levels and its impact on fecal metabolites, fecal samples were treated with cold 80% methanol for 4 h at 4°C. Samples were then centrifuged at 14,000 g for 20 min at 4°C. Supernatants were transferred to a sterile 1.5 mL tube and stored at −80°C. Bacterial supernatants were treated with 4X volume of the 80% methanol. Polar metabolomic analysis was performed by the WCM Proteomics and Metabolomics Core for target polar metabolomics analysis by LC-MS. Metabolites were identified using an in-house library established using chemical standards. Identification required exact mass (within 5ppm) and standard retention times. To determine short chain fatty acids (SCFAs) fecal levels, target metabolomics were performed using liquid chromatography–quadruple–time of flight mass spectrometry as previously described.[64] Relative metabolite quantitation was performed based on peak area for each metabolite evaluated and normalized by sample weight.

16S rRNA sequencing

To evaluate if the fecal microbiome of patients were efficiently transplanted into germ-free mice, both patient-donors and mice fecal samples were subjected to 16S rRNA sequencing at WCM Microbiome Core Facility. Briefly, after DNA isolation, the 16S V4 and V5 regions were amplified as previously described (https://earthmicrobiome.org). Amplicons were then sequenced in an Illumina MiSeq platform using the 2 × 250 bp paired-end protocol. Read pairs were processed using DADA2[65] with forward truncation length of 240, reverse truncation length of 160, and otherwise default parameters, VSEARCH,[66] and the SILVA Database[67] (version 138) for taxonomic assignment. This produced a rarefied amplicon sequence variant (ASV) tables and phylogenetic tree (sequence depth of 12000 reads for human data and 10146 reads for mouse data) for downstream microbiome analysis. 16S rRNA seq analyses were performed in R studio (Boston, MA). Beta diversity was calculated using R package 'phyloseq'[68] based on unweighted uniFrac, while plots were constructed in 'ggplot2' or GraphPad (San Diego, CA).

In vitro assays and bacterial RNA-seq

F. prausnitzii ATCC 27768 or *E. rectale* DSM 17629 was grown at 37°C, anaerobically in YCFAC media (for transcriptomics) or RCM media (for metabolomics) with sodium hydroxide (NaOH) vehicle control (0.5M; Sigma-Aldrich, St. Louis, MO), sulfapyridine (500, 1000, 2000μM; Sigma-Aldrich, St. Louis, MO) and/or folate (566μM; Sigma-Aldrich, St. Louis, MO), adapted from Nayak et al., 2021.[38] CFU from *F. prausnitzii* cultures were assessed anaerobically in YCFA agar. Growth was measured by absorbance, OD_{600}, on SpectraMax Plus (Molecular Devices, San Jose, CA). RNA isolation was performed using RNeasy PowerMicrobiome kit (Qiagen, Hilden, Germany) following the manufacture instructions. RNA was then quantified by Nanodrop prior to reverse transcription with qScript cDNA SuperMix kit (Quantabio, Beverly, MA) or RNAseq library preparation.

RNA-seq library preparation and sequencing were performed by WCM Genomics Core. For library preparation, the Illumina Stranded Total RNA Prep kit was used. High-throughput sequencing was performed using the PE 2x50 cycles protocol in the NovaSeq 6000 Illumina platform targeting 10 million reads/sample. Bioinformatics and statistical analysis were then performed by the WCM Bioinformatics Core. Samples were aligned with STAR[69] to NCBI reference genome GCF_000154385.1 (*F. prausnitzii* M21/2). Quality control was performed with QoRTs[70] on aligned BAM files. Counts per gene were then calculated using featureCounts.[71] BioCyc[72] analyses were performed with clusterProfiler to identify pathways/gene sets that are overrepresented among the differentially expressed genes.

Quantitative RT-PCR

qPCR was performed on an Applied BioSciences Quant Studio 6 Flex Real-time PCR (Applied Biosystems, Waltham, MA) using PerfeCTa SYBR Green Fast mix, Low ROX (Quantabio, Beverly, MA). The following primers were used: for 16S rRNA gene −515F 5′ GTGYCAGCMGCCGCGGTAA 3′, −926R 5′ CCGYCAATTYMTTTRAGTTT 3′[51]; *F. prausnitzii but* gene F: 5′ GTGGATGCCTTTGT GGATATTG 3′, R: 5′ CCGGGTTATCGTTCAGGTAATC 3′ and *E. rectale but* gene F: 5′ CTCAGCAGATGAGGCAGTAAAG 3′, R: 5′ GGAAGCTCTGAGTAACGGATTG 3' (designed on the PrimerQuest Tool from IDT, Coralville, IA). The thermocycler program was as

follows: initial cycle of 95°C for 60 s, followed by 40 PCR cycles at 95°C for 5 s, 60°C for 15 s, 72°C for 15 s. Relative levels of the *but* target gene was determined by calculating the Δ Ct to the conserved 16S rRNA gene expression.

QUANTIFICATION AND STATISTICAL ANALYSIS

For endpoint analysis, Fisher's exact test implemented in JMP 14 (SAS Institute Inc., Cary, NC) was used when proportions were compared between binary variables. To determine significance of categorical variables, Student's t test was applied if two groups were compared, otherwise two-way ANOVA test was used. For non-parametric data, Wilcoxon matched-pairs signed-rank test was calculated when paired analyses were carried, otherwise Mann-Whitney test was applied. If required, Bonferroni or Tukey tests were applied for multiple comparison correction. Metagenomic and transcriptomic analyses were performed in R studio (Boston, MA) using R package 'phyloseq'[68] and plots were constructed in 'ggplot2' or GraphPad (San Diego, CA). Differential gene expression analysis was performed with DESeq2.[73] Differential taxa or pathway abundance was assessed using linear discriminant analysis (LDA) effect size (LEfSe).[31] Correlation between two continuous variables (e.g., fecal drug levels, Δ BASDAI, alpha diversity) was determined with linear regression models. For discriminating responders from non-responders, we fit linear regression models on the relative abundances of select taxa and constructed corresponding ROC curves. Area under the curve (AUC) and *p* values were computed using R.